Applied Surface Science Advances 15 (2023) 100407

Contents lists available at ScienceDirect

Applied Surface Science Advances

journal homepage: www.sciencedirect.com/journal/applied-surface-science-advances

Reduced graphene oxide/silver nanoparticles/β-cyclodextrin nanosponges composites with improved photocatalytic activity

Antonella Di Vincenzo [a], Delia Chillura Martino [a], Elena Piacenza [a], Pellegrino Conte [b], Alberto Pettignano [c], Giuseppe Lazzara [c], Paolo Lo Meo [a,*]

[a] Dipartimento di Scienze e Tecnologie Biologiche, Chimiche e Farmaceutiche (STEBICEF), Università di Palermo – V.le delle Scienze, ed. 17, 90128 Palermo, Italy
[b] Dipartimento di Scienze Agrarie, Alimentari e Forestali (SAAF), Università di Palermo – V.le delle Scienze, ed. 4, 90128 Palermo, Italy
[c] Dipartimento di Fisica e Chimica - Emilio Segrè (DiFC), Università di Palermo – V.le delle Scienze ed. 17, 90128 Palermo, Italy

ARTICLE INFO

Keywords:
Cyclodextrin
Graphene oxide
Nanosponges
Photodegradation
Silver nanoparticles

ABSTRACT

Significant activity improvement was achieved by associating graphene oxide-silver composite photocatalysts with cyclodextrin-based nanosponge materials, due to the synergistic effect provided by the supramolecular host abilities of the nanosponge. Three photocatalysts were prepared, fully characterized (FT-IR, ss-NMR, Raman, XRD, SEM, EDX, AFM, ICP, TGA, potentiometric titration), and tested for the oxidative photodegradation of some dyes and phenols, chosen as model organic pollutants. Compared to the unsupported photocatalyst, the nanosponge-based materials showed enhanced performances (being able to carry out the degradation even of dyes which do not react in the presence of the unsupported catalyst), and good recyclability. The activity improvement is attributed to a local concentration effect provided by the nanosponge, able to capture the organic substrate in the proximity of the actual photocatalyst. The results presented herein provide a helpful basis for designing advanced catalytic systems.

1. Introduction

Process sustainability in industrial and environmental applications requires the design and development of catalysts with high efficiency and, possibly, selectivity. Therefore, modern research has addressed the study of composite systems, joining diverse and mutually integrating functions. According to the Aristotelian idea that "*the whole is something besides the parts*", synergism between different functional moieties may result in significantly improved performances. In particular, great attention has been paid in the last years to the combination of "ordinary" catalysts with supporting materials having supramolecular host abilities. Nanosponges (NSs) [1] provide in this context very interesting cases of study. These materials are hyper-cross-linked polymers made up of supramolecular host macrocycles (cyclodextrins in the most common cases) joined through of suitable linker units. They can be easily prepared via quite simple organic reaction routes. Different "generations" of NSs have been considered [2] according to their possible functionalization, which can be introduced either by a sensible choice of linkers [3–4] or by a chemical post-modification [5] of a preformed material. Hence, stimuli-sensitive materials can be obtained [6], whose physicochemical properties can be tuned up as a function of the environmental conditions [7–8]. This can be particularly useful in view of possible applications as drug carrier/delivery systems [9–14] or environmental remediation devices [15]. There are some reports in recent literature describing the use of NSs as supports for noble metal (Ag, Au, Rh, Pd) nanoparticle catalysts (NP) [16], in order to improve catalytic performances towards some model reactions (nitroarene reduction, C—C and N—N coupling reactions, hydrogenation). The resulting NS/NP composites exploit the adsorption ability of the NS material towards the substrate undergoing the catalytic reaction, concentrating it near the NP catalytic center.

As long as environmental remediation problems are concerned, such as wastewaters treatment, the photodegradation of organic pollutants constitutes an interesting, quite effective and relatively low-cost tool. Photooxidation processes require the use of a photocatalyst and atmospheric O_2 as the sacrificial oxidant. Graphene-based materials have attracted large attention in this context, due to their versatility. The general mechanisms involved are quite well understood [17–19]. Photoexcitation causes the formation of a hole-e^- couple, ultimately resulting in the formation of hydroperoxide radical species, able to

* Corresponding author.
E-mail address: paolo.lomeo@unipa.it (P. Lo Meo).

https://doi.org/10.1016/j.apsadv.2023.100407
Received 5 November 2022; Received in revised form 20 April 2023; Accepted 30 April 2023
Available online 2 May 2023

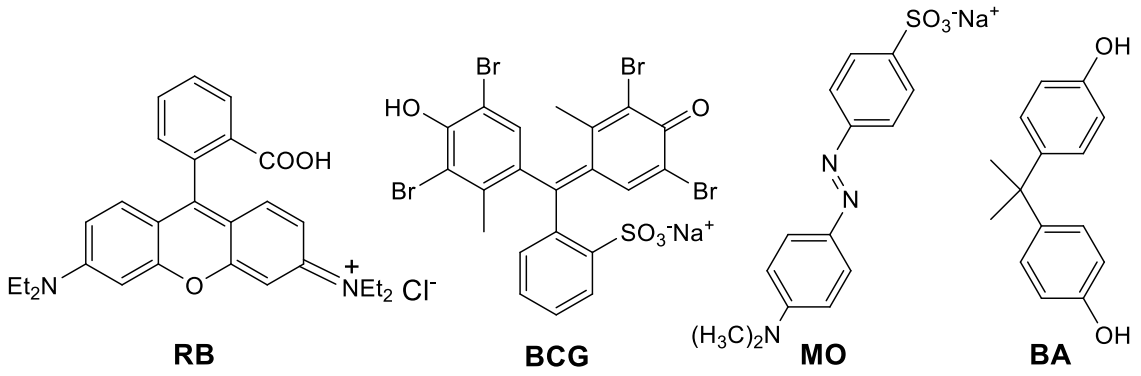

Fig. 1. Structures of the model pollutants and dyes.

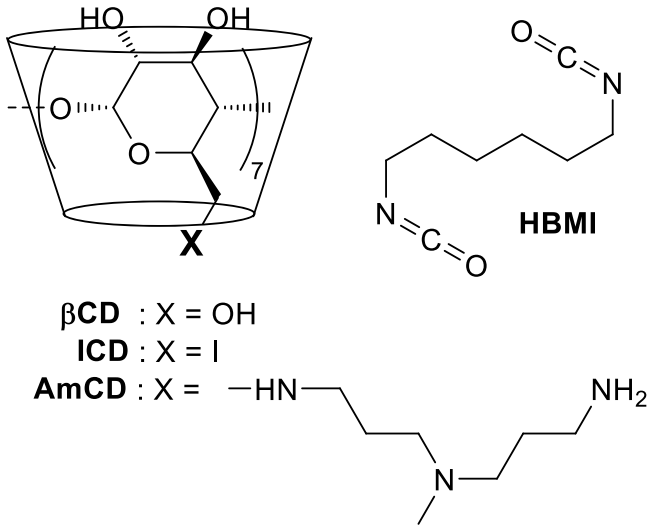

Fig. 2. Structures of βCD, BrCD, AmCD and HBMI.

initiate the oxidative degradation of the organic pollutant molecule. Recently, systems based on reduced graphene oxide (RGO) conjugated with silver nanoparticles (AgNPs) have been found very effective for this purpose [20–26]. In particular, Divya et al. [27], Naz et al. [28], Li et al. [29], Chandu et al. [30] and Pretheesia et al. [31] have reported very interesting results on testing them in the photodegradation of model dyes such as Rhodamine B or Methylene blue.

Besides, the adsorption of organic dyes by nanosponges has been largely reported in recent literature [32–34]. In particular, we have been interested in the synthesis and pH-tunable adsorption and release properties of diverse nanosponges materials (namely, mixed cyclodextrin-calixarene NSs [5,8,35], polyamino-cyclodextrin NSs [3], polyamino-calixarene NSs [36–37]), and in their possible association with nanostructured catalysts, such as silver nanoparticles [16]. Therefore, in the present work the possibility to support RGO/AgNPs composites into nanosponge architectures was explored. The idea of chemically joining graphene derivatives with cyclodextrins has been occasionally explored in recent literature [38–40]. The present study aims at showing how the supramolecular binding abilities of nanosponges in capturing suitably structured organic aromatic substrates, acts in synergism with the photoactive species, thereby enabling to achieve improved photodegradation efficiencies as compared to the plain photocatalyst. Two different systems were designed, where RGO/AgNPs composites are embedded in either a polyurethane-cyclodextrin or a polyamino-cyclodextrin NS matrix. These systems, indicated hereinafter as M1 and M2, were compared with an unsupported RGO/AgNP photocatalyst (indicated hereinafter as RGOAg) similar to the ones considered in the aforementioned studies [27–31]. The efficiency of these photocatalysts was then tested towards some model pollutants and dyes, namely Rhodamine B (RB), Bromocresol Green (BCG), Methylorange (MO) and Bisphenol A (BA) (Fig. 1).

2. Materials and methods

2.1. Materials and instrumentation

All reagents needed (Cyclolab, Aldrich, Merck) were used as purchased with no further purification. Anhydrous β-cyclodextrin (βCD, purchased from Cyclolab (HU)) was obtained by drying the commercial hydrate product in vacuo over P_2O_5 at 90 °C overnight. The heptakis-(6-deoxy)-(6-iodo)-β-cyclodextrin (ICD) and the poly-(6-deoxy)-{6-[(N-methyl-N-(3-amino-propyl)−3-amino]−1-propylamino}-β-cyclodextrin (AmCD, Fig. 2) were synthesized as described elsewhere [41–43].

UV–Vis spectra were recorded on a Beckmann Coulter DU 800 spectrophotometer equipped with a Peltier thermostatic apparatus. ATR-FTIR spectra were acquired on a Bruker LUMOS instrument. CP-MAS solid-state NMR spectra were recorded on a Bruker Avance II 400 MHz spectrometer. Thermogravimetric analyses were performed on a TA Instruments TGA Q5000 apparatus under a nitrogen flux; samples were heated up to 900 °C at a 2.5 °C/min rate. ICP-OES analyses were performed on a Perkin Elmer Model Optima 2100 apparatus. SEM micrographs and EDX images/spectra were acquired on a JEOL JEMES-2100 instrument. Raman spectra were acquired on a Horiba LabRAM HR Evolution apparatus using a 532 nm laser source. X-ray diffraction (XRD) patterns were collected using a Philips PW 1050/39 diffractometer (Philips Analytical, Almelo, The Netherlands) with Bragg Brentano geometry, equipped with a Ni-filtered Cu Kα radiation source and operated at 40 kV and 30 mA (step 0.1°; counting time 5 s/step); patterns were collected in the 2θ range between 10° and 70° The obtained XRD patterns were processed and analyzed using the Match! Software (Crystal Impact) and the linked Crystallography Open Database (COD). AFM images were acquired on a Bruker FastScan Bio apparatus.

2.2. Preparation of GO and its derivatives

2.2.1. Pristine graphene oxide (pGO)

The pristine pGO product was prepared according to a modified Hummers procedure. In details, graphene (1.04 g), $NaNO_3$ (0.52 g, 6.1 mmoles) and conc. H_2SO_4 (23 mL, 429 mmoles) were mixed at 0 °C under vigorous stirring, then solid $KMnO_4$ (3.02 g, 19.1 mmoles) was cautiously added in small portions. The mixture was kept under stirring for 2 h at 0 °C and subsequently warmed at 35 °C in 30 min. Then, H_2O (46 mL) was added and the system stirred at 90 °C for 50 min. After a short cooling, further water (140 mL) and 30% H_2O_2 (3 mL) were added, and the mixture allowed to settle at r.t. for 3 days. The precipitated solid was decanted and treated with conc. HCl (20 mL) at r.t. overnight. The solid was separated and repeatedly washed with warm water (70 °C);

Table 1
Results of photodegradation tests.

entry	catalyst	substrate	mg of catalyst per 10 mL	Initial conc. (ppm)	Time (h)	% of degraded substrate	light source
1	RGOAg	BA	4	40	5	32 ± 2	halogen lamp
2	RGOAg	RB	2	5	2	17 ± 1	halogen lamp
3	RGOAg	BCG	2	5	2	–	halogen lamp
4	RGOAg	MO	2	5	2	–	halogen lamp
5	M1	BA	40	40	5	10 ± 1	halogen lamp
6	M1	RB	20	5	1	19 ± 1	halogen lamp
7	M1	RB	20	5	2	20 ± 1	halogen lamp
8	M1	RB	20	5	3	21 ± 1	halogen lamp
9	M1	BCG	20	5	2	22 ± 1	halogen lamp
10	M1	MO	20	5	2	24 ± 1	halogen lamp
11	M1	RB	20	5	2	–	Blue LED 467 nm
12	M1	RB	20	5	2	16 ± 1	Green LED 513 nm
13	M1	RB	20	5	2	14 ± 1	Red LED 627 nm
14	M1	RB	20	5	2	15 ± 1	NIR LED 860 nm
15	M2	BA	10	40	5	–	halogen lamp
16	M2	RB	10	5	2	29 ± 2	halogen lamp
17	M2	BCG	10	5	2	95 ± 3	halogen lamp
18	M2	MO	10	5	2	77 ± 3	halogen lamp

then, it was suspended again in cold water (110 mL) and cautiously treated with $NaHCO_3$ up to neutrality. The final product was centrifuged, washed with methanol (twice) and diethyl ether (twice), dried overnight in vacuo over P_2O_5 at 60 °C, and crunched in a mortar. Yield 1.20 g.

2.2.2. Reduced graphene oxide (RGO)

pGO (200 mg) was suspended in water (15 mL) and treated with an excess $NaBH_4$ (200 mg, 5.28 mmoles). The mixture was allowed to stir at r.t. for 30 min; then HCl 1 M was added dropwise up to neutrality. The solid was centrifuged, washed with methanol (twice) and diethyl ether (twice), dried overnight in vacuo over P_2O_5 at 60 °C, and finally crunched in a mortar. Yield 198 mg.

2.2.3. Hydrolized graphene oxide (hGO)

To pGO (240 mg) suspended in methanol (5 mL) NaOH (200 mg, 5.0 mmoles) was added, and the mixture was allowed to stir at r.t. under inert atmosphere (Ar) for 24 h. Then, HCl 1 M was added dropwise up to acidic pH (ca. 3.0); the solid was collected by centrifugation, washed with methanol (twice) and diethyl ether (twice), dried overnight in vacuo over P_2O_5 at 60 °C, and crunched in a mortar. Yield 173 mg.

2.2.4. Acetylated graphene oxide (aGO)

pGO (100 mg) was suspended in a mixture of dry pyridine (1 mL) and acetic anhydride (3 mL) and the mixture was stirred at 65 °C under inert atmosphere (Ar) for 24 h. The system was then poured into ethyl acetate (20 mL); then, the crude product was vacuum filtered and rapidly washed with methanol acidulated with a little HCl. The product was finally collected, dried overnight in vacuo over P_2O_5 at 60 °C, and crunched in a mortar. Yield 75 mg.

2.2.5. Reduced graphene oxide/silver nanoparticles composite (RGOAg)

pGO (214 mg) was dispersed in water (15 mL) by brief sonication, and solid $AgNO_3$ (339 mg, 2 mmoles) was dissolved into the suspension. Then $NaBH_4$, (75 mg, 2 mmoles) was added, and the mixture was kept under vigorous stirring at r.t. for 30 min. The system was allowed to settle overnight, then the supernatant liquor was decanted off. The solid was washed with methanol (twice) and diethyl ether (twice) and filtered off. Yield 401 mg.

2.3. Synthesis of material M1

Anhydrous βCD (283 mg, 0.25 mmoles) and RGOAg composite (40.5 mg) from the previous preparation were carefully mixed in a mortar. The obtained powder was introduced into a little vial, then a solution was added obtained by dissolving hexamethylene-bis-isocyanate (HMBI, see Fig. 2; 120 μL, 126 mg, 0.75 mmoles) in DMSO (250 μL). The system was mechanically mixed with a tiny metal rod to obtain a paste which was allowed to react still at 60 °C for 20 h. The crude solid obtained was grossly crunched and transferred into a centrifuge tube with methanol (30 mL), shortly sonicated and centrifuged. The product was again washed with methanol (30 mL) and then with diethyl ether (twice, 30 mL each). Finally, the solid was dried overnight in vacuo over P_2O_5 at 60 °C, crunched in a mortar and passed through a 150 μm sieve. Yield 282 mg. A sample of a polyurethane-βCD NS material analogous to M1 without the RGOAg composite was prepared according to literature [44] for useful comparison, using the same cyclodextrin/HMBI mole-to-mole ratio.

2.4. Synthesis of material M2

The ICD (260 mg, 0.136 mmoles), AmCD (274 mg, 0.124 mmoles) and pGO (81 mg) were carefully mixed in a mortar. The powder mixture was transferred in a little vial, DMSO (300 μL) was added, and the system was mechanically stirred with a tiny metal rod to obtain a paste, which was allowed to react still at 60 °C for 48 h. The gummy crude formed was then washed twice with methanol and twice with diethyl ether as described hereinabove, to obtain a precursor solid material that was dried, crunched in a mortar and passed through a 150 μm sieve. This material was subsequently suspended in water (3 mL), $AgNO_3$ (250 mg, 1.47 mmoles) was added, and the system was allowed to stir in the dark for 1 h. Then, excess $NaBH_4$ (200 mg, 5.28 mmoles) was added to the suspension, and the system was stirred for further 30 min. The solid product was centrifuged, washed with methanol and diethyl ether, and finally dried as described previously. Yield 518 mg. A sample of the polyamino-cyclodextrin NS material analogous to M2 was prepared according to literature [3,16] for useful comparison.

2.5. Potentiometric titrations

2.5.1. pGO and hGO

A carefully weighed amount of substance (ca. 40 mg) was suspended by sonication in 12.0 mL of freshly double distilled and degassed water; then, 3.0 mL of standard HCl 0.1 M were added. The suspension was then titrated with a standard NaOH 1.0 M solution, introduced in small portions by means of a Chemetron screw microsyringe. The pH value of the suspension was determined, after each addition of the titrant, by means of a common pH-meter, and the obtained titration curve was subjected to regression analysis according to literature [41–42], using the proper equation obtained analytically for the mixture of one strong acid with two weak bases.

Table 2
Recycling results of the M2 catalyst using RB.

cycle	1	2	3	4	5	6	7	8	9
degradation %	29 ± 1	16 ± 1	20 ± 1	24 ± 1	30 ± 1	31 ± 1	30 ± 1	32 ± 1	23 ± 1

2.5.2. aGO

A carefully weighed amount of substance (ca. 25 mg) was suspended by sonication in 2 mL of MeOH, and then 1 mL of standard NaOH 1.0 M was added. The mixture was kept under inert atmosphere (Ar) and gentle stirring at 60 °C for 24 h, in order to accomplish the hydrolysis of all the ester and lactone groups. Then, the mixture was cooled to r.t. and 12 mL of standard HCl 0.1 M were added. The obtained suspension was then titrated with NaOH 1.0 M, and analytical data were subjected to regression analysis, as described above.

2.6. ICP analyses

A carefully weighed amount (ca. 5.00 mg) of silver containing material was placed in a small ceramic crucible and mineralized with HNO_3 (ca. 2 mL) at 90 °C up to complete decomposition. The residue was dissolved in freshly double distilled water and diluted up to 100 mL. The obtained solution was filtered through a 0.45 μm Millipore membrane before analysis by Inductively Coupled Plasma Emission Spectroscopy (ICP-OES) technique by using a PerkinElmer Model Optima 2100, equipped with an autosampler model AS-90.

2.7. Photodegradation experiments

The proper amount (see Section 3.2, Table 1) of photocatalyst was mixed in a vial with a solution (10 mL) of the organic substrate dissolved in Milli-Q grade water (18.2 MΩ·cm) at the proper concentration (namely, 5.0 ppm for RB, BCG and MO, 40.0 ppm for BA). The sample was allowed to equilibrate in the dark for 30 min; then, it was irradiated in a homemade apparatus constituted by a box, having the internal walls covered in tin foil, and a 50 W halogen lamp placed in such a way to provide an irradiation power as large as 275 W/m^2. Irradiation was maintained for the proper time while stirring was achieved by mounting the described apparatus on an orbital shaker plate. After the proper irradiation time, the sample was centrifuged to separate the photocatalyst, and the residual amount of substrate was determined by UV–Vis spectrophotometry. Experiments with LED irradiation were performed in a similar way, by simply substituting the light source and maintaining the same irradiation power. All the experiments were performed in the presence of no buffer, after having checked that pH variation was negligible. In order to gain the correct estimation of the catalytic activity, the amount of unreacted adsorbed dye was evaluated. In detail, the catalyst recovered from the photodegradation experiment was repeatedly washed with small portions (i.e. 1 mL) of methanol till washings appeared colorless (three or four passages were usually sufficient; at each passage, the photocatalyst was recovered by centrifugation at 13,000 rpm for 10 min). The collected liquors were diluted up to 10 mL, and the obtained solution was analyzed by UV–vis spectrophotometry to determine the residual dye concentration. Finally, the overall amount of unreacted dye was obtained by trivial stoichiometric calculations. Photodegradation data reported in Tables 1 and 2 are averaged over three replicates.

For the reuse tests, the photocatalyst recovered from the previous experiment was dried in vacuo at 60 °C overnight, carefully weighed, and re-suspended in the suitable amount of fresh dye solution, in such a way to keep constant the catalyst-to-solution (w/v) ratio, namely 1 mL of solution per 1 mg of catalyst.

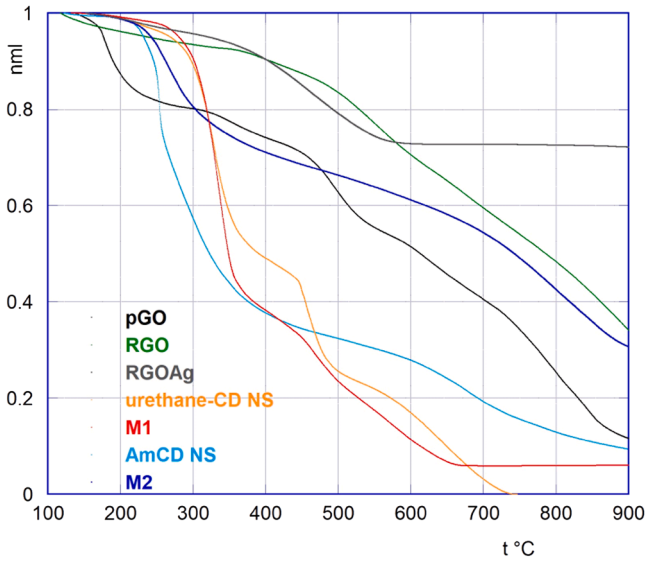

Fig. 3. TGA curves of the photocatalysts and their precursors and reference materials.

3. Results and discussion

3.1. Characterization of the materials

As a preliminary remark, it must be noted that the preparation of the model RGOAg composite used in this study was designed in analogy with the most performing material among those described by Divya et al. [27]. These authors found that a 50:50 w/w silver-GO ratio ensured the most effective photodegradation of RB. Material M1 was designed in order to have a way to have the RGOAg composite merely dispersed within the polyurethane-cyclodextrin NS matrix, in a 10% amount in weight. For material M2, it was considered that plain polyamino-cyclodextrin NSs are able to sequestrate the Ag^+ ions from aqueous solution up to a significant extent [16], and that the adsorbed Ag^+ immediately undergoes reduction by treatment with $NaBH_4$ to afford the expected metal nanoparticles. Therefore, a precursor made by the polyamino-cyclodextrin NS matrix loaded with a 15% amount in weight of pGO was first prepared. Then, the precursor was allowed to equilibrate with an excess of Ag^+, and finally the system was treated with the $NaBH_4$ reducing agent in order to form in situ the AgNPs. It is worth stressing here that silver nanoparticles in M1 are specifically bound to the graphene surface; conversely, such a strict association is not compelled in M2.

The three photocatalysts obtained were preliminarily characterized by ICP analysis, in order to determine their actual metal loadings. In detail, silver contents as large as 45 ± 2% for RGOAg, 4.0 ± 0.4% for M1 and 15.6 ± 0.5% for M2 were found. Hence, the loading for the Divya's-like RGOAg composite resulted slightly lower than the theoretical expected 50%. It is worth noting that in the reference work [27] no independent evaluation of the actual loading after the synthesis has been reported. Indeed, the occurrence of minor losses of silver during work-up procedures is reasonable, as accounted for by the typical reddish color of the first washing liquors. This idea is confirmed by the analysis of material M1. The physical embedding of the pre-formed RGOAg composite into the NS matrix involves a further small metal loss, hardly significant within the experimental errors. Regarding the material M2, the observed loading is significantly lower than expected (i.e. ca. 20.8%, calculated considering that the analogous material not loaded with pGO has been reported to have a 24.5% silver loading [16]). This can be partly attributed to the loss of AgNPs that occurs in the washing steps, as accounted for again by the fact that the first washing liquors showed the typical reddish color of nanoparticle silver.

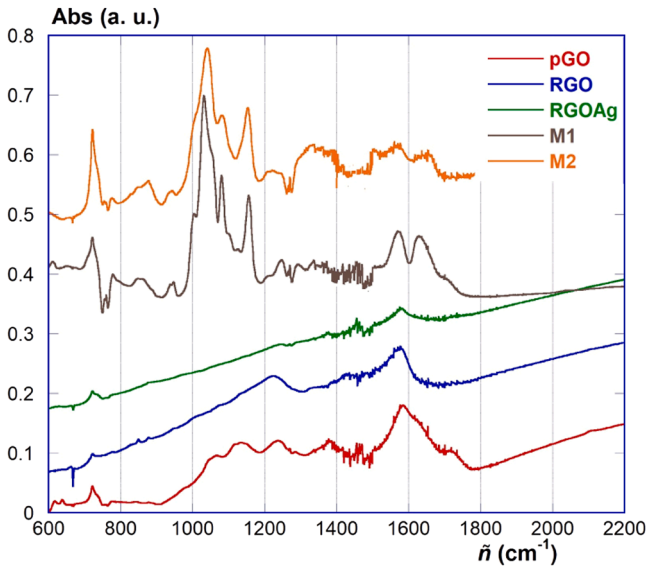

Fig. 4. ATR-FTIR spectra (curves have been suitably offset for clarity).

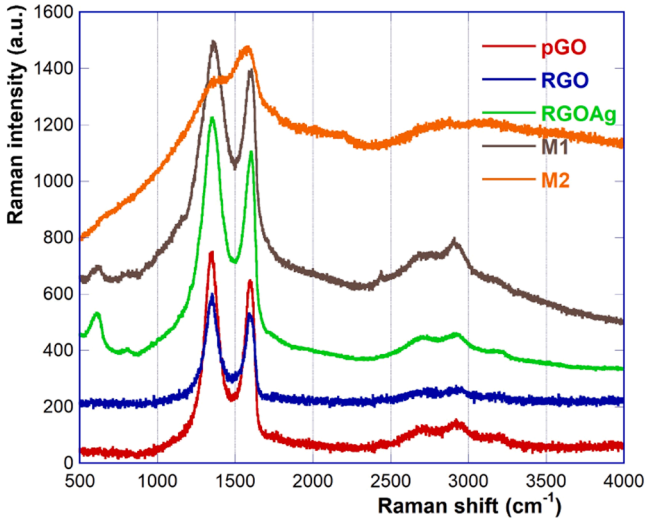

Fig. 5. Raman spectra (curves have been suitably rescaled and offset for clarity).

Further useful information was obtained by means of a thermogravimetric (TGA/DTG) [45–46] analysis, aimed also at verifying the thermal stability of the materials. The complete collection of TGA curves is depicted in Fig. 3. The starting pGO shows a fairly complex TGA curve, with two main degradation steps at 177 °C and 495 °C, and a final 11.7% residue at 900 °C. Borohydride reduction leading to RGO causes a significant variation in the degradation profile, according to a much smoother curve, the slope of which significantly increases at 500 °C; a final 34.6% residue at 900 °C is found. For RGOAg, the TGA curve features a main decomposition step at 458 °C, with a final residue at 900 °C as large as 72.1%. Considering that the metal contribution to thermogravimetric is null, by trivial algebraic passages, a 42.7% silver content can be estimated for RGOAg, in reasonable agreement with the results from the ICP analysis.

The comparison of the TGA curves of materials M1 and M2 with those of the relevant plain NSs, again evidenced the effect of the metal loading. The reference plain polyurethane-cyclodextrin NS, which M1 is based on, shows a degradation profile with three main steps at 330 °C, 458 °C and 645 °C, and a complete degradation above 750 °C. The M1 curve shows a main apparent step at 335 °C (comparable to the first step of the plain NS), and a second smoother one up to the plateau above 680 °C, leaving a final 6.0% residue. Again, the metal loading that can be calculated from these results, namely 4.3%, is in reasonable agreement with the ICP result. Similarly, the TGA profiles of the plain polyaminocyclodextrin NS and the relevant composite M2 show significant differences. The former features two main decomposition steps at 253 and 286 °C, and a third shallow one centered at 678 °C, with a 9.7% final residue. Conversely, M2 shows a first decomposition step at 267 °C and a shallow second one at ca. 806 °C, with a 30.9% final residue. Keeping into account the theoretical RGO/AmCD weight ratio used in the preparation of the material, from the mass residues at 900 °C a silver content as large as 20.0% can be estimated, once again in reasonable agreement with the ICP results.

The analytical characterization of the pGO material was completed by a titrimetric determination of the ionizable groups present (a typical example is depicted in the Supporting Information, Figure S1). The obtained titration curve was subjected to fitting analysis by using the proper equation algebraically obtained [36,41] for a mixture of two independent virtual bases. The obtained regression parameters confirmed the presence of two different types of ionizable groups, having p*K*a values as large as 5.16 ± 0.06 (0.93 ± 0.03 meq/g) and 9.13 ± 0.05 (1.11 ± 0.03 meq/g), which can be easily identified as carboxyl and phenolic groups respectively. Similarly, for more detailed characterization, the titrimetric approach was exploited to estimate the amount of non-phenolic hydroxyl groups and lactone groups. For this purpose, two further samples were prepared, the first one (hGO) obtained by alkaline hydrolysis of the pristine pGO, and the second by acetylation (aGO) of pGO and subsequent alkaline hydrolysis under mild conditions. Also for these samples, titration curves can be analyzed using the two weak acids model. A smart combination of the analytic results obtained (see Supporting Information for mathematical details) leads to estimate the presence of 0.36 ± 0.05 meq/g of non-phenol hydroxyl groups and 0.41 ± 0.05 meq/g of lactone groups. Further oxygenated groups (epoxide, aldehyde or ketone) were not quantified.

Spectroscopic characterization of the materials was based on ATR-FTIR and Raman spectroscopy. In general, the FTIR spectra (Fig. 4) of the graphene-based materials are difficult to acquire because of the strong background absorption due to the low-energy electronic transitions of the largely conjugated carbon backbone. Considering the diagnostic 2000~1000 cm^{-1} region, the spectrum of the precursor GO features a characteristic series of signals centered at 1722 cm^{-1} (C = O str.), 1583 and 1383 cm^{-1} (C = C str.), 1238, 1133 and 1067 (C—O str.) cm^{-1}. After borohydride reduction, the spectrum of RGO lacks the C = O and most of the C—O signals, showing only the 1577 and 1383 cm^{-1} signals (C = C str., the latter one being very shallow) and a further peak at 1228 cm^{-1} (C—O str.). The presence of Ag in RGOAg nanoparticles causes a strong broadband absorption in the IR region, making the entire spectrum almost unreadable.

The spectra of the composites basically show the signals expected for the nanosponge backbone, which largely overlap with the relatively weak signals of the graphene derivatives. In particular, in the aforementioned spectral region, the typical cyclodextrin fingerprint band system (1155, 1078, 1028, 1005, 944 cm^{-1}) is apparent, together with the graphene band at 1572 cm^{-1}. Moreover, the M1 spectrum also features a signal at 1627 cm^{-1} (with a shoulder at ca 1700 cm^{-1}) accounting for the presence of the urethane linker functional groups. A signal at 1650 cm^{-1} (NH bending) can be found in the spectrum of M2.

The Raman spectra (Fig. 5) of the same materials provide further information. The spectra feature the well-known systems of bands in the ranges 1100–1700 cm^{-1} (given by the superimposition of the D*, D, D", G and D' bands) and 2400–300 cm^{-1} (with the 2D and S3 bands). In particular, the amount of structural defects and the extent of the graphene-like domains, as well as the number of graphene layers [46–51], can be related by the intensity ratios between the D and G bands (I_D/I_G), the 2D and G bands (I_{2D}/I_G), and the 2D and S3 bands

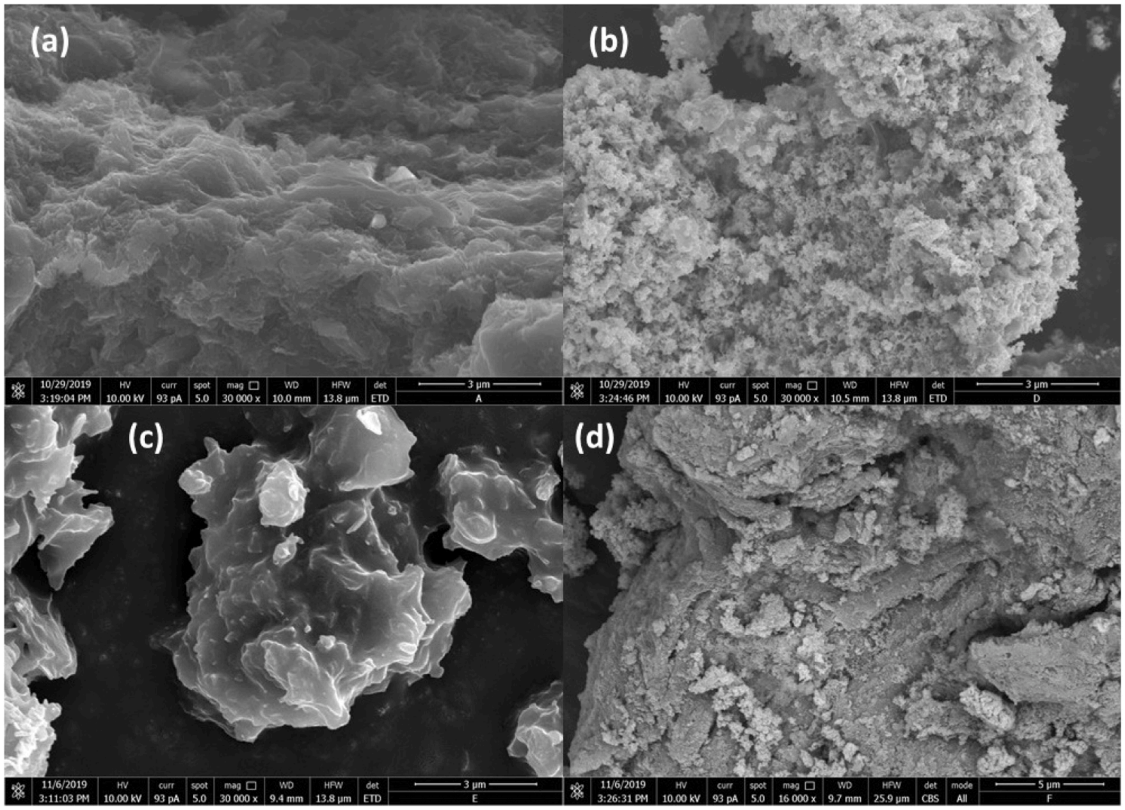

Fig. 6. SEM micrographs of pGO (a), RGOAg (b), M1 (c) and M2 (d). The reference line represents a 3 μ length in (a-c) and 5 μ in (d).

(I_{2D}/I_{S3}). These ratios can be obtained after the proper deconvolution analyses (complete graphs are collected in the Supporting Information, Figures S2). In particular, the I_D/I_G value decreases from 4.11 for pGO to 3.51 for RGO, and then it increases to 6.08 and 6.27 for RGOAg and M1 respectively. A similar trend can be found for the I_{2D}/I_G value, passing from 0.74 for pGO to 0.69 for RGO, 0.97 for RGOAg and 1.64 for M1. Moreover, the I_{2D}/I_{S3} value increases from 1.02 for pGO to 1.13 for RGO, to 1.31 for RGOAg and to 1.79 for M1. Noticeably, the silver containing materials feature also a tiny signal centered at 611 cm^{-1}. These results suggest that the materials obtained are mixtures of few-layered rather than single-layered sheets; however, increasing exfoliation likely occurs, due to mechanical and chemical stress, on passing from the pristine pGO to the silver-containing materials RGOAG and M1. The presence of single and multi-layered sheets is confirmed by AFM images (see Supporting Information, Figures S5 for some representative image). Interestingly, deconvolution analysis could not be performed for material M2, because the spectrum appears poorly resolved and superimposed to a sort of wide absorption band. This anomalous finding might be related to the peculiar structure of the material, in particular to the possible presence of silver nanoparticles not bound to the graphene layers, but directly interacting with the N atoms present in the polyamine linker subunits of the AmCD nanosponge. Indeed, polyamino-cyclodextrins strongly bind the Ag^+ ion, forming complexes that easily undergo photoreduction to form silver nanoparticles [52], and this process is specifically promoted by green light (513 nm) [43]. Keeping into account that a 532 nm laser source was used for spectra acquisition, the occurrence of anomalous absorption effects of the excitation radiation seems then reasonable.

In order to achieve completeness, it is worth mentioning here that $^{13}C(^1H)$ CP-MAS Solid State NMR characterization of the plain polyurethane-cyclodextrin and polyamino-cyclodextrin nanosponges had already been performed and reported [3,44]. In detail, these spectra present the signals expected for the cyclodextrin moieties, namely at ca. 103 ppm (C1), 83 ppm (C4), 72 ppm (cumulatively C2, C3 and C5), 61 ppm (C6). Moreover, the spectra feature broad signals relevant to the linker chains centered at ca. 50 ppm (aliphatic C bound to N) and 26 ppm (aliphatic C not bound to N). The spectra of the composite materials M1 and M2 are almost superimposable to those of the uncharged nanosponges, confirming the existence of the cross-linked polymer network. However, possible signals relevant to the graphene carbons are hardly detectable in the spectra. This can be easily explained considering that these C atoms cannot benefit from the cross-polarization enhancing effect, because they are not directly bound to H atoms.

The characterization of the materials was completed by SEM and XRD techniques. Some significant SEM micrographs are reported in Fig. 6.

The pristine pGO (Fig. 6a) appears as a mass of microsheets tightly stuck together. These sheets appear densely covered in silver nanocrystals on passing to RGOAg (Fig. 6b). Material M1 (Fig. 6c) appears as a compact mass, given by the polyurethane nanosponge matrix; nevertheless, the presence of the graphene microsheets embedded beneath the surface can be envisaged. Conversely, M2 presents an even more compact, and somehow stiffer, appearance, with tiny silver nanoparticles that can be spotted on its surface (Fig. 6d; a SEM image of the material after reuse was also acquired, see later).

XRD patterns of pGO and RGO (see Supporting Information, Figure S6) show several peaks attributable to residual Na_2SO_4 (COD 900–4093) from the materials workup procedure. Besides, pGO features a diffraction peak centered at 12.3° corresponding to the (001) plane, providing further confirmation about the successful introduction of oxygen-containing functional groups in the graphene sheets [53]. Indeed, oxygen functionalities cause structural defects and surface roughness on the original graphene sheets, which, in turn, determines an enlargement of the inter-planar distance between GO sheets [54]. Furthermore, the position and intensity of the peak referring to the (001) plane vary with the amount of water molecules adsorbed onto GO sheets [55]. The low-intensity peak at 12.3° observed for pGO suggests that the GO obtained through procedure adopted here is relatively dry (i.e., it has

a low amount of adsorbed water) [55]. After reduction, a shift of the 12.3° peak to 24.3° was detected in RGO, which refers to the (002) plane of graphene [46,54]. This evidence corroborates the removal of oxygen-containing groups from GO and the reduction of the graphene sheets inter-spacing [53]. Specifically, the broadening of the RGO peak at 24.3° indicates the restoration of the conjugated sp^2 carbon network and the generation of randomly ordered graphene platelets [54]. Moreover, pGO and RGO XRD patterns display a peak corresponding to the (100) plane of the hexagonal carbon structure centered at 42.5°, which is sharper in the former and infers a short-range order of stacked graphene layers [56].

Conversely, RGOAg shows three intense diffraction peaks at 38.1°, 44.2°, and 64.4°, which corresponds to the (111), (200) and (220) planes of face centered cubic crystal AgNPs (COD 9012961) [50], confirming the formation of highly crystalline Ag on the RGO surface. Finally, the absence of the RGO (002) peak can indicate GO complete exfoliation deriving from the AgNP formation and growth on the graphene sheets, preventing their approaching and restacking [57].

3.2. Photocatalytic activity

A preliminary efficiency assessment for the plain RGOAg photocatalyst, aimed at an useful comparison with the cited work by Divya et al. [27], was carried out towards Rhodamine B (RB). The cited Authors reported an almost quantitative degradation for a 1 ppm solution of the dye after 2 h of irradiation under visible light in the presence of their own RGOAg photocatalyst (20 mg per 100 mL of dye solution). In the present case, it was considered more convenient to work with a more concentrated dye solution (5.0 ppm), using the same catalyst weight/-solution volume ratio (according to ICP data, this corresponds to the presence of 0.78 mmoles/L of Ag, compared with the theoretical 0.93 mmoles/L of Ag of the reference work [26]). The plain RGOAg composite prepared in this study apparently showed a similar activity as compared with Divya's results; in fact, after 2 h of irradiation, ca. 91% of the dye apparently disappeared. However, taking into account the well-known adsorption abilities of graphene derivatives towards organic substances, the possible presence of unreacted RB adsorbed onto the photocatalyst was checked. Therefore, the catalyst was recovered by centrifugation after the photodegradation experiment, and then washed with methanol. It was actually found that ca. 74% of the initial dye could be recovered unchanged. Thus, one can conclude that only a 17% amount of dye actually undergoes photodegradation under the operational conditions. It must be mentioned that a similar counter-check was not reported in the reference work [27]. Hence, actual neat photodegradation yields were calculated by keeping into account the amount of unreacted substance eluted (MeOH) after the photoirradiation experiment. Further tests with the title RGOAg composite revealed a fair activity only towards Bisphenol A, though under slightly modified conditions, i.e. starting from a 40 ppm solution, 4 mg of photocatalyst per 10 mL of solution and 300 min irradiation. Disappointingly, RGOAg was found inactive towards Bromochresol Green (BCG) and Methyl Orange (MO). It is worth noting that RGOAg in the dark is able to adsorbe quite effectively RB (88%) and MO (47%), whereas negligible adsorption is found for BA and BG. The whole of the results obtained with the three materials is summarized in Table 1.

Considering materials M1 and M2, operational conditions were set to have an amount of silver in the reaction sample roughly comparable with that present in the case of RGOAg. Therefore, 20 mg of photocatalyst per 10 mL of solution were generally used in the case of M1 and 10 mg per 10 mL in the case of M2. As long as M1 is concerned, decreased activity towards BA (only 10% of photodegradation, under the same conditions) was observed with respect to plain RGOAg. Conversely, activity towards dyes is quite interesting, because a significant degradation was observed after 2 h irradiation with both dyes BCG (22%) and MO (24%). Regarding RB, degradation after 2 h showed only a minor increase with respect to RGOAg. However, tests at different times showed that there is anyway a significant effect on reaction rates. In fact, after only 1 h irradiation a 19% degradation was observed (slightly increased up to 21% after 3 h). Again, these results can be easily related to the ability of material M1 to absorb the different substrates in the dark. In fact, under the same concentration conditions, for dyes RB, MO and BCG the adsorption percentages are 52%, 64% and 89%, respectively, but only 15% for BA. This positively outlines the favorable effect of the ability of the photocatalyst to interact with the organic substrate, that can reasonably lead back to a local concentration effect, as mentioned in the Introduction.

Indeed, based on the adsorption percentages reported hereinabove, it can be roughly estimated that the concentration of the dye within the NS phase is ca. three orders of magnitude larger than in solution. The apparently unfavorable effect towards BA can be related to its scarce adsorption, which in turn leads back to its scarce affinity for the cyclodextrin cavity. This is consistent with the fact that shape and polarization complementarity is important in host-guest supramolecular interactions [58–60]. Unlike dyes, which have a flat, largely conjugated and polarizable molecular structure, the bent and almost apolar molecule of BA cannot effectively interact with the host subunits.

The effect due to the NS matrix is even more apparent on passing to material M2. In fact, due to the presence of the polyamine chain linkers, which are partly protonated even under neutral pH conditions, the NS backbone is positively charged. This enhances the electrostatic effects affecting the adsorption properties of the material. It can be preliminarily observed that M2 adsorbs BA up to a negligible extent; conversely, adsorptions for dyes RB, MO and BCG are as large as 68%, 78% and 77%, respectively. Consistently, no photodegradation was observed for BA, whereas a further improvement was observed for the degradation of dyes, resulting as large as 29% for RB, 77% for MO, up to an outstanding 95% for BCG. Care is needed in evaluating the latter results because the actual amount of silver present in the system must be kept into account, i.e. 0.080 mg/mL and 0.156 mg/mL for M1 and M2, respectively. Hence, after suitable normalization of the results, it is interesting to notice that degradation of cationic RB is non enhanced at all, whereas significant enhancement occurs for anionic MO and BCG. These observations are in perfect agreement with the aforementioned cationic nature of the M2 material backbone, which, of course, favors the interaction with anionic species.

Further insights were gained by examining the effect of the light source. In particular, the degradation of RB with M1 was performed in the presence of some LED sources, under the same reaction and irradiation power conditions. Interestingly, no degradation was induced by blue radiation (467 nm); conversely degradation was observed in the presence of green (513 nm), red (627 nm) and NIR (860 nm) radiation, although slightly lesser performances (15%) occur in comparison with the use of polychromatic halogen lamp. These observations outline the existence of a lower wavelength limit for the induction of the electron transfer process involved in the photodegradation reactions. Noticeably, this limit corresponds to the wavelength at which the photoreduction of Ag^+ ion and the formation of silver nanoparticles is induced in the presence of polyaminocyclodextrins [43].

Finally, the possible recyclability of the materials was verified. In particular, the reuse of material M2 in the photodegradation of RB was tested. This material was used up to nine reaction cycles. At each cycle, the catalyst suffered only minor mass losses during recovering (less than 3%). This led to an overall 80% mass recover at the ninth cycle. Normalized results obtained keeping into account these losses are summarized in Table 2.

Data show a peculiar trend. In fact, a significant drop in activity can be observed after the first use. Then, activity is progressively recovered in the subsequent reuses; however, it drops again at the ninth cycle. This complex trend can be justified in terms of wearing out of the material. In details, after the first use, a non-negligible amount of the silver loading is lost, as accounted for by the fact that the UV–vis spectrum of the aqueous solution, recovered after the photoirradiation experiment,

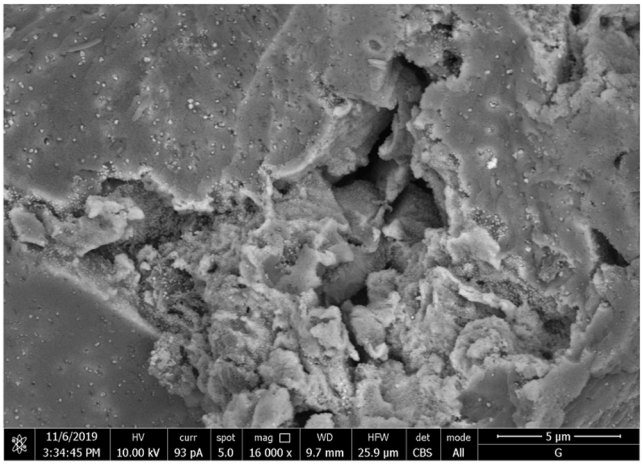

Fig. 7. SEM micrographs M2 after nine reuse cycles (the reference line represents a 5 µ length).

presents the typical surface plasmon resonance band of nanoparticle silver centered at 420 nm. It can be reasonably hypothesized that relatively loosely bound AgNPs residing on the surface of the photocatalyst grains (which are well visible in SEM micrographs) are mechanically lost during the process. The subsequent activity recover can be attributed to the gradual mechanical fragmentation of the material in the various reuses, which increases the surface exposed to the solution, thereby improving the permeability and the exchange ability of the nanosponge. However, this mechanism works until further loss of actual photocatalyst occurs. Loss of silver load can be clearly envisaged by comparison of the SEM micrographs of freshly prepared M2 (Fig. 5d) and after nine reuse cycles (Fig. 7). In fact, Ag nanoparticles on the surface appear much sparser on the surface of the nanosponge support, which in turn shows a fair mechanical wearing.

Loss of surface silver loading was further assessed by means of EDX analysis. Relevant micrographs (see Supporting Information, Figures S3 and S4) show the presence of areas with a lower amount of metal. Interestingly, EDX spectra (see Supporting Information, Figures S3 and S5) show also a significant presence of iodine in the pristine M2, which is largely lost after the reuse cycles. The presence of iodide ions in the material is a consequence of the synthetic procedure (namely, of the use of ICD as starting material [3]). Of course, I^- ions are easily washed away from the material during its use.

4. Conclusions and further remarks

In this study, the photodegradation of some model molecules mediated by Ag nanoparticles and reduced graphene oxide photocatalyst supported into cyclodextrin nanosponge architectures was explored. The results presented herein positively assess the efficiency enhancement of the catalytic performances, due to joining the photoactive material with the functional support, which is achieved by exploiting the supramolecular host abilities of the latter system. In particular, the degradation of dyes such as BCG and MO was achieved with the composite materials M1 and M2; this is not observed with the plain RGOAg. The nanosponge, indeed, is able to concentrate the substrate near the photoactive species. Further advantages in using the composite systems undoubtedly derive from the easier recoverability of the material, which can be reused for several cycles, although performances appear to be significantly affected by the mechanical stress underwent by the material and the progressive loss of the silver load. From a methodological standpoint, the results presented herein also outline the fact that care is needed in evaluating the actual performances of photocatalysts, able to establish strong supramolecular interactions with the substrate, as accounted for by the case of the plain RGOAg material. In these cases, indeed, a correct evaluation of the activity requires to keep into account the amount of substrate adsorbed onto the material that has not actually undergone degradation. Finally, the poor performances towards BA can be led back to its scarce affinity for the nanosponges used. The latter finding outlines the importance of a correct design of the supporting nanosponge, which can even be suitably optimized up to achieve selectivity for a given substrate.

Declaration of Competing Interest

The authors declare that they have no known competing financial interests or personal relationships that could have appeared to influence the work reported in this paper.

Data availability

Data will be made available on request.

Acknowledgments

SiciliAn MicronanOTecH Research And Innovation CEnter “SAMOTHRACE” (MUR, PNRR-M4C2, ECS_00000022), spoke 3 - Università degli Studi di Palermo “S2-COMMs - Micro and Nanotechnologies for Smart & Sustainable Communities is gratefully acknowledged for financial support. Raman experimental data were provided by the “Raman Spectroscopy Lab of ATeN Center - Università di Palermo”; prof. S. Agnello is gratefully acknowledged for support. Sem micrographs were acquired at the “Electron Microscopy Lab of ATeN Center - Università di Palermo”; prof. V. La Carrubba is gratefully acknowledged for support. AFM images were acquired at the “Surfaces, Thin films and Devices Lab of ATeN Center - Università di Palermo”; prof. G. Buscarino is gratefully acknowledged for support.

Supplementary materials

Supplementary material associated with this article can be found, in the online version, at doi:10.1016/j.apsadv.2023.100407.

References

[1] Nanosponges: Synthesis and Applications, Wiley-VCH Verlag GmbH & Co. KGaA, Weinheim, Germany, 2019.
[2] F. Caldera, M. Tannous, R. Cavalli, M. Zanetti, F. Trotta, Int. J. Pharm. 531 (2017) 470–479, https://doi.org/10.1016/j.ijpharm.2017.06.072.
[3] M. Russo, M.L. Saladino, D. Chillura Martino, P. Lo Meo, R. Noto, RSC Adv. 6 (2016) 49941–49953, https://doi.org/10.1039/c6ra06417e.
[4] F. Castiglione, V. Crupi, D. Majolino, A. Mele, W. Panzeri, B. Rossi, F. Trotta, V. Venuti, J. Incl. Phenom. Macrocycl. Chem. 75 (2013) 247–254, https://doi.org/10.1007/s10847-012-0106-z.
[5] V. Cinà, M. Russo, G. Lazzara, D. Chillura Martino, P. Lo Meo, Carbohydr. Polym. 157 (2017) 1393–1403, https://doi.org/10.1016/j.carbpol.2016.11.018.
[6] F. Trotta, F. Caldera, C. Dianzani, M. Argenziano, G. Barrera, R. Cavalli, Chempluschem 81 (2016) 439–443, https://doi.org/10.1002/cplu.201500531.
[7] S. Cataldo, P. Lo Meo, P. Conte, A. Di Vincenzo, D. Milea, A. Pettignano, Carbohydr. Polym. 267 (2021), 118151, https://doi.org/10.1016/j.carbpol.2021.118151.
[8] A. Di Vincenzo, M. Russo, S. Cataldo, D. Milea, A. Pettignano, P. Lo Meo, ChemistrySelect 4 (2019) 6155–6161, https://doi.org/10.1002/slct.201901200.
[9] R.M. Fontana, N. Milano, L. Barbara, A. Di Vincenzo, G. Gallo, P. Lo Meo, ChemistrySelect 4 (2019) 9743–9747, https://doi.org/10.1002/slct.201902373.
[10] S. Guernelli, A. Cariola, A. Baschieri, R. Amorati, P.Lo Meo, Mater. Adv. 1 (2020) 2501–2508, https://doi.org/10.1039/D0MA00566E.
[11] V. Coviello, S. Sartini, L. Quattrini, C. Baraldi, M.C. Gamberini, C.La Motta, Eur. J. Pharm. Biopharm. 117 (2017) 276–285, https://doi.org/10.1016/j.ejpb.2017.04.028.
[12] P. Pandey, D. Purohit, H. Dureja, Recent Pat Nanotechnol. 12 (2018) 180–191, https://doi.org/10.2174/1872210512666180925102842.
[13] S. Allahyari, F. Trotta, H. Valizadeh, M. Jelvehgari, P. Zakeri-Milani, Expert Opin. Drug Del. 16 (2019) 467–479, https://doi.org/10.1080/17425247.2019.1591365.
[14] M. Massaro, V. Cinà, M. Labbozzetta, G. Lazzara, P. Lo Meo, P. Poma, S. Riela, R. Noto, RSC Adv. 6 (2016) 50858–50866, https://doi.org/10.1039/C6RA06143E.

[15] N. Morin-Crini, G. Crini, Prog. Polym. Sci. 38 (2013) 344–368, https://doi.org/10.1016/j.progpolymsci.2012.06.005.
[16] M. Russo, A. Spinella, A. Di Vincenzo, G. Lazzara, M.R. Correro, P. Shahgaldian, P. Lo Meo, E. Caponetti, ChemistrySelect 4 (2019) 873–879, https://doi.org/10.1002/slct.201803424.
[17] R. Gusain, K. Gupta, P. Joshi, O.P. Khatri, Adv. Colloid Interface Sci. 272 (2019), 102009, https://doi.org/10.1016/j.cis.2019.102009.
[18] W.S. Koe, J.W. Lee, W.C. Chong, Y.L. Pang, L.C. Sim, Environ. Sci. Poll. Res. 27 (2020) 2522–2565, https://doi.org/10.1007/s11356-019-07193-5.
[19] S. Naz, Q. Mansoor, A. Nisar, S. Karim, M. Khan, G. Ali, A. Rahman, M. Ahmad, ChemistrySelect 4 (2019) 8372–8377, https://doi.org/10.1002/slct.201901124.
[20] D.B. Thinh, N.M. Dat, N.N.K. Tuyen, L.T. Tai, N.D. Hai, N.T. Tinh, L.M. Huong, T. Do Dat, Q.T.T. Huong, N.T.H. Nam, D.T.Y. Oanh, M.T. Phong, N.H. Hieu, Vietnam J. Chem. 60 (2022) 553–570, https://doi.org/10.1002/vjch.202200034.
[21] N. Zhang, Y. Zhang, Y.-J. Xu, Nanoscale 4 (2012) 5792–5813, https://doi.org/10.1039/C2NR31480K.
[22] G. Mamba, G. Gangashe, L. Moss, S. Hariganesh, S. Thakur, S. Vadivel, A.K. Mishra, G.D. Vilakati, V. Muthuraj, T.T.I. Nkambule, J. Environ. Chem. Eng. 8 (2020), 103505, https://doi.org/10.1016/j.jece.2019.103505.
[23] M. Hasanpour, M. Hatami, J. Mol. Liq. 309 (2020), 113094, https://doi.org/10.1016/j.molliq.2020.113094.
[24] P.V.L. Reddy, K.-.H. Kim, B. Kavitha, V. Kumar, N. Raza, S. Kalagara, J. Environ. Manag. 213 (2018) 189–205, https://doi.org/10.1016/j.jenvman.2018.02.059.
[25] K. He, Z. Zeng, A. Chen, G. Zeng, R. Xiao, P. Xu, Z. Huang, J. Shi, L. Hu, G. Chen, Small 14 (2018), 1800871, https://doi.org/10.1002/smll.201800871.
[26] M.E. Khan, M.M. Khan, M.H. Cho, Nanoscale 10 (2018) 9427–9440, https://doi.org/10.1039/C8NR03500H.
[27] K.S. Divya, A. Chandran, V.N. Reethu, S. Mathew, Appl. Surf. Sci. 444 (2018) 811–818, https://doi.org/10.1016/j.apsusc.2018.01.303.
[28] S. Naz, Q. Mansoor, A. Nisar, S. Karim, M. Khan, G. Ali, R. Ata ur, M. Ahmad, Chemistryselect 4 (2019) 8372–8377, https://doi.org/10.1002/slct.201901124.
[29] X. Li, J. Natsuki, T. Natsuki, Environ. Technol. Innov. 21 (2021), 101210, https://doi.org/10.1016/j.eti.2020.101210.
[30] B. Chandu, C.M. Kurmarayuni, S. Kurapati, H.B. Bollikolla, Carbon Lett 30 (2020) 225–233, https://doi.org/10.1007/s42823-019-00091-3.
[31] T. Pratheesya, S. Harish, N. M, S. Sohila, R. Ramesh, Mater. Res. Expr. 6 (2019), 074003, https://doi.org/10.1088/2053-1591/ab1567.
[32] M.T. Sikder, M.M. Rahman, M. Jakariya, T. Hosokawa, M. Kurasaki, T. Saito, Chem. Eng. J. 355 (2019) 920–941, https://doi.org/10.1016/j.cej.2018.08.218.
[33] S. Iravani, R.S. Varma, Appl. Sci. 12 (2022), https://doi.org/10.3390/app12094182.
[34] P. Kumari, P. Singh, A. Singhal, Environ. Sci. Poll. Res. 27 (2020) 32432–32448, https://doi.org/10.1007/s11356-020-09519-0.
[35] P. Lo Meo, G. Lazzara, L. Liotta, S. Riela, R. Noto, Polym. Chem. 5 (2014) 4499–4510, https://doi.org/10.1039/C4PY00325J.
[36] A. Spinella, M. Russo, A. Di Vincenzo, D. Chillura Martino, P. Lo Meo, Beilstein J. Org. Chem. 14 (2018) 1498–1507, https://doi.org/10.3762/bjoc.14.127.
[37] A. Di Vincenzo, A.P. Piccionello, A. Spinella, D. Chillura Martino, M. Russo, P. Lo Meo, Beilstein J. Org. Chem. 15 (2019) 633–641, https://doi.org/10.3762/bjoc.15.59.
[38] H. Tian, H. Zeng, F. Zha, H. Tian, Y. Chang, Water Air Soil Poll. 231 (2020) 495, https://doi.org/10.1007/s11270-020-04865-8.
[39] A. Heydari, H. Sheibani, V. Hronský, I. Janigová, M. Šlouf, P. Šiffalovič, I. Chodák, Chem. Papers 72 (2018) 1299–1313, https://doi.org/10.1007/s11696-017-0371-9.
[40] S. Kumar, M.M. Rahman, S. Yoon, S.M. Mamun Kabir, J. Koh, Inorg. Nano-MetalChem 50 (2020) 286–291, https://doi.org/10.1080/24701556.2019.1711124.
[41] P. Lo Meo, F. D'Anna, M. Gruttadauria, S. Riela, R. Noto, Carbohydr. Res. 347 (2012) 32–39, https://doi.org/10.1016/j.carres.2011.10.029.
[42] M. Russo, D.La Corte, A. Pisciotta, S. Riela, R. Alduina, P.Lo Meo, Beilstein J. Org. Chem. 13 (2017) 2751–2763, https://doi.org/10.3762/bjoc.13.271.
[43] M. Russo, D.C. Martino, E. Caponetti, P.Lo Meo, ChemistrySelect 3 (2018) 3048–3055, https://doi.org/10.1002/slct.201703098.
[44] P. Lo Meo, F. Mundo, S. Terranova, P. Conte, D. Chillura Martino, J. Phys. Chem. B 124 (2020) 1847–1857, https://doi.org/10.1021/acs.jpcb.9b11935.
[45] L.M. Huong, C.Q. Cong, N.M. Dat, N.D. Hai, N.T.H. Nam, H. An, L.T. Tai, T. Do Dat, N.T. Dat, M.T. Phong, N.H. Hieu, J. Cleaner Prod. 392 (2023), 136269, https://doi.org/10.1016/j.jclepro.2023.136269.
[46] T.T. Buu, V.H. Son, N.T.H. Nam, N.D. Hai, H.-.T. Vuong, L.T.K. Quang, N.M. Dat, T. H. Lin, M.T. Phong, N.H. Hieu, Ceram. Int. 49 (2023) 9868–9882, https://doi.org/10.1016/j.ceramint.2022.11.162.
[47] F. Yin, S. Wu, Y. Wang, L. Wu, P. Yuan, X. Wang, J. Solid State Chem. 237 (2016) 57–63, https://doi.org/10.1016/j.jssc.2016.01.015.
[48] A.Y. Lee, K. Yang, N.D. Anh, C. Park, S.M. Lee, T.G. Lee, M.S. Jeong, Appl. Surf. Sci. 536 (2021), 147990, https://doi.org/10.1016/j.apsusc.2020.147990.
[49] F.T. Johra, J.-.W. Lee, W.-.G. Jung, J. Ind. Eng. Chem. 20 (2014) 2883–2887, https://doi.org/10.1016/j.jiec.2013.11.022.
[50] S.P. Dubey, M. Lahtinen, M. Sillanpää, Process Biochem 45 (2010) 1065–1071, https://doi.org/10.1016/j.procbio.2010.03.024.
[51] B. Tang, H. Guoxin, H. Gao, Appl. Spectrosc. Rev. 45 (2010) 369–407, https://doi.org/10.1080/05704928.2010.483886.
[52] M. Russo, A. Meli, A. Sutera, G. Gallo, D. Chillura Martino, P. Lo Meo, R. Noto, RSC Adv. 6 (2016) 40090–40099, https://doi.org/10.1039/c6ra00042h.
[53] H. Saleem, M. Haneef, H.Y. Abbasi, Mater. Chem. Phys. 204 (2018) 1–7, https://doi.org/10.1016/j.matchemphys.2017.10.020.
[54] J. Shen, Y. Hu, M. Shi, X. Lu, C. Qin, C. Li, M. Ye, Chem. Mater. 21 (2009) 3514–3520, https://doi.org/10.1021/cm901247t.
[55] G.K. Yogesh, E.P. Shuaib, P. Roopmani, M.B. Gumpu, U.M. Krishnan, D. Sastikumar, Diamond Relat. Mater. 104 (2020), 107733, https://doi.org/10.1016/j.diamond.2020.107733.
[56] L. Stobinski, B. Lesiak, A. Malolepszy, M. Mazurkiewicz, B. Mierzwa, J. Zemek, P. Jiricek, I. Bieloshapka, J. Electron. Spectrosc. Relat. Phenom. 195 (2014) 145–154, https://doi.org/10.1016/j.elspec.2014.07.003.
[57] T. Kavinkumar, K. Varunkumar, V. Ravikumar, S. Manivannan, J. Colloid Interf. Sci. 505 (2017) 1125–1133, https://doi.org/10.1016/j.jcis.2017.07.002.
[58] F. D'Anna, P. Lo Meo, S. Riela, M. Gruttadauria, R. Noto, Tetrahedron 57 (2001) 6823–6827, https://doi.org/10.1016/S0040-4020(01)00635-4.
[59] P. Lo Meo, F. D'Anna, S. Riela, M. Gruttadauria, R. Noto, Tetrahedron 65 (2009) 2037–2042, https://doi.org/10.1016/j.tet.2009.01.008.
[60] M.V. Rekharsky, Y. Inoue, Chem. Rev. 98 (1998) 1875–1918, https://doi.org/10.1021/cr970015o.